Chalcogenide Letters Vol. 22, No. 6, June 2025, p. 529 - 540

Electronic structure, optical properties, and elastic properties of solar material $CuInSe_2$ from theoretical simulation

T. J. Li [a,*], Y. Yue [a], L. P. Qu [a], H. J. Hou [b], S. H. Fan [b], H. L. Guo [c]
[a] *Institute of Automotive and Traffic Engineering, Yancheng Polytechnic College, Yancheng 224005, China*
[b] *School of Materials Engineering, Yancheng Institute of Technology, Yancheng, 224051, China*
[c] *College of Electronic and Information Engineering, Yangtze Normal University, Fuling, 408000, Chongqing, China*

This work uses the theoretical method to calculates and analyzes a series of properties of the crystal such as electronic structure, optical properties, and elastic constants. The results show that the optimized structural parameters of the $CuInSe_2$ is close to the experimental values. The analysis of various parameters of optical properties shows that the crystal is transparent for incident light with energy greater than 25 eV. Furthermore, the calculation of elastic constants reveals that $CuInSe_2$ exhibits significant anisotropy and possesses excellent ductility.

(Received March 24, 2025; Accepted June 13, 2025)

Keywords: $CuInSe_2$, Electronic structure, Optical, Elastic properties

1. Introduction

In the early stage, the most studied solar cells were those related to a-Si and CdTe [1-2]. However, amorphous silicon solar cells are not suitable for long-term use due to the light-induced degradation effect, and cadmium telluride is restricted in use due to its lack of environmental protection characteristics. In contrast, $CuInSe_2$ and its derivatives $Cu(In, Ga)Se_2$ have achieved a laboratory conversion efficiency of over 20.3%[3-5]. Gurel et al. employed the adiabatic bond charge model to investigate and compute the lattice dynamics properties of several chalcopyrite compounds [6]. Kushwaha performed a comprehensive analysis of phonon frequencies and elastic characteristics for six ternary chalcopyrite semiconductors, employing the rigid ion model as the computational framework [7]. Jose J. Plata conducted a theoretical study examining the thermal conductivity across a series of 20 chalcopyrite semiconductors [8]. Although there have been some studies on $CuInSe_2$, we found that the above-mentioned studies are still not systematic. This study investigates the physical characteristics of $CuInSe_2$ through DFT calculations.

* Corresponding author: litj1021@126.com
https://doi.org/10.15251/CL.2025.226.529

2. Calculation method

The physical properties computations were performed utilizing the CASTEP simulation package [9]. The Perdew-Burke-Ernzerhof Generalized Gradient Approximation (PBE-GGA) functional was selected for the calculations [10]. The atomic electrons are modeled using ultra-soft pseudopotentials and the calculations are performed [11]. For the structure calculations, the cutoff energy of the plane wave in inverse *k*-space is 400.0 eV. The calculations guarantee a high degree of convergence in all parameters: the accuracy is controlled to within 2×10^{-6} eV/atom. The Brillouin zone *k*-vector of the band structure is chosen to be 4×4×2.

3. Results and discussion

3.1. Structural properties

$CuInSe_2$ has a chalcopyrite structure. This structure is composed of two face-centered cubic lattices. One is the anion Se element, and the other is composed of the cations of Cu and In elements. Based on x-ray diffraction data, the lattice constants at room temperature are $a = b = 5.78$ Å, $c = 11.59$ Å [12]. The calculated internal coordinate parameter *u* and lattice constants *a* and *c* are listed in Table 1. The crystal structural of $CuInSe_2$ is shown in Fig. 1. The obtained lattice constants are: $a = b = 5.773$Å, $c = 11.5590$Å. The computed outcomes align well with both experimental data and theoretical predictions [12-14], indicating the reliability of our calculation.

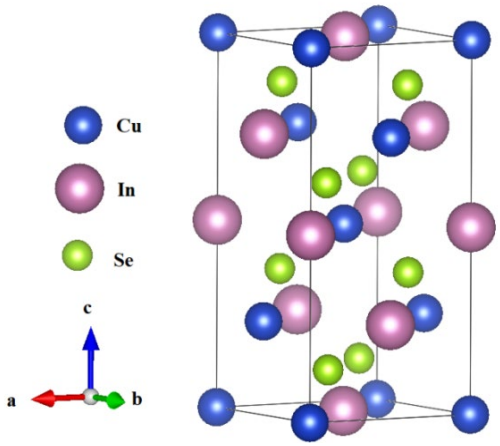

Fig. 1. The chalcopyrite unit cell structure of $CuInSe_2$.

Table 1. Lattice constants (a, c) (Å) and internal coordinate parameter u of $CuInSe_2$.

Parameters	This work	Theo.[13]	Exp.[12]	Exp.[14]
a/Å	5.773	5.770	5.784	5.873
c/Å	11.5590	11.5530	11.616	11.583
u	0.22	-	-	-

3.2. Electronic properties

Fig. 2 illustrates the band structure of $CuInSe_2$. In Fig. 2, there are many and dense energy level curves in the valence band between -5 and 0 eV. The calculated band gap is E_g = 1.016 eV, and the $CuInSe_2$ belongs to a semiconductor.

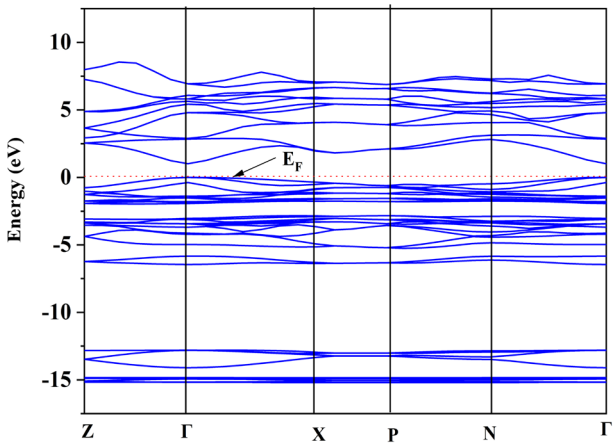

Fig. 2. Energy band structure of $CuInSe_2$.

Fig. 3 illustrates density of states (DOS) for $CuInSe_2$. The electronic structures of $CuInSe_2$ atoms are: Cu $3d^{10}4s^1$, In $5s^25p^14d^{10}$, Se $4s^24p^4$. The three regions in the figure show that: within -15.8 to -12.3 eV, the DOS of $CuInSe_2$ is mainly contributed by the 4s state electrons of Se; within -6.7 to 1 eV, the DOS is mainly contributed by the 4p orbital electrons of Se atoms; within 2 to 8.3 eV, the contribution to the DOS mainly comes from the p orbital electrons of Cu. The DOS associated with the higher-energy valence band primarily originates from the interaction between the 3d electrons of Cu and the 4p electrons of Se.

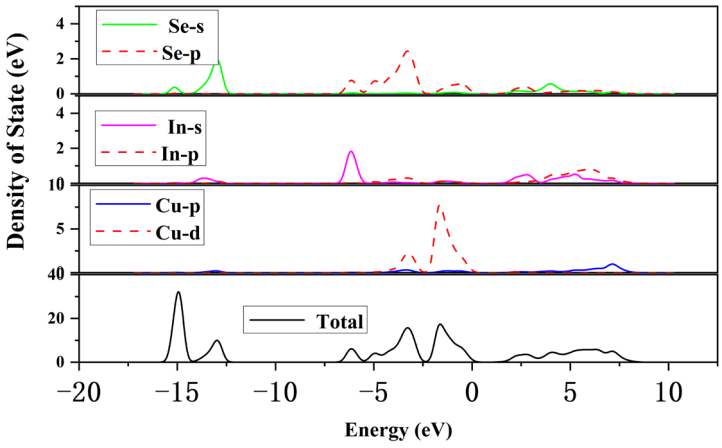

Fig. 3. Total and partial DOS of $CuInSe_2$.

3.3. Optical properties

The relative dielectric function of a substance with light absorption can be expressed as complex numbers [15]

$$\varepsilon(\omega) = \varepsilon_1(\omega) + i\varepsilon_2(\omega) \tag{1}$$

Fig. 4 shows the variation curves of real part ε_1 and imaginary part ε_2. The intersection of the real part ε_1 with the vertical axis is $\varepsilon_1(0) = 10.6$. The real part curve first rises slightly, reaches a maximum value at about 2.5 eV, and then decreases rapidly with the increase of frequency, then rises slowly and finally tends to be horizontal. ε_1 is negative in the range of 7-16 eV. The imaginary part curve ε_2 increases rapidly with it initially rises with increasing incident light energy, then gradually declines before stabilizing. At about 12 eV, ε_2 decreases to 0.

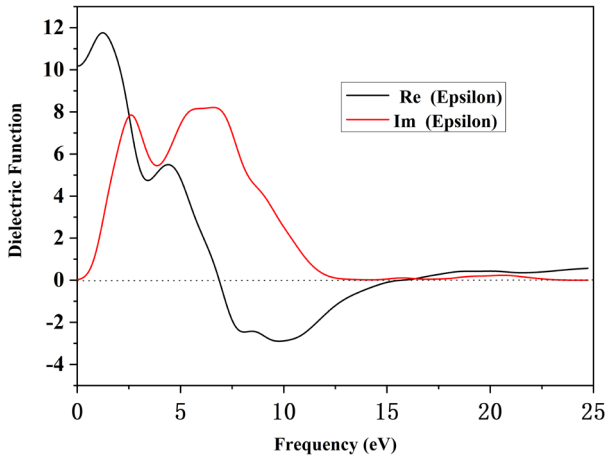

Fig. 4. ε_1 and ε_2 of $CuInSe_2$.

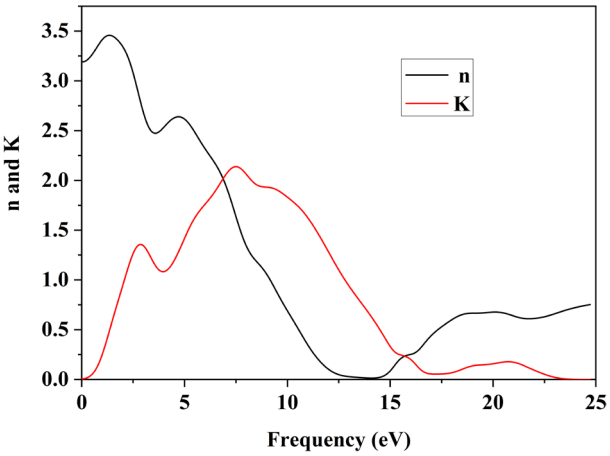

Fig. 5. n and k of $CuInSe_2$.

In Fig.5, the refractive index $n(\omega)$ with the vertical axis is $n_0 = 3.2$. The maximum refractive index is near 2 eV, and the figure indicates that the peak refractive index reaches approximately 3.45. Then the refractive index decreases as the incident light energy increases, reaches a minimum value (about zero) near 14 eV, and then gradually increases. The extinction coefficient k gradually increases with the increase of the incident light energy, reaches a peak near 8 eV, and then decreases approximately symmetrically. The extinction coefficient drops to zero for incident light energies exceeding 23 eV.

Combining Figs.4-5, the relationships between ε_1, $n(\omega)$, and $k(\omega)$ are

$$\varepsilon_1 = n^2(\omega) - k^2(\omega) \tag{2}$$

When $n(\omega) < k(\omega)$, $\varepsilon_1 < 0$. The ε_1 is negative in the range of about 7-16 eV, the corresponding wave vector is an imaginary number, and the refractive index is very small. Therefore, it can be concluded that light in the range of 7-16 eV cannot propagate in the $CuInSe_2$.

The absorption coefficient is

$$\alpha(\omega) = \frac{\omega\varepsilon_2(\omega)}{cn(\omega)} \tag{3}$$

When $n(\omega)$ is not equal to zero, the absorption coefficient is directly related to ε_2. The absorption spectrum of $CuInSe_2$ is illustrated in the figure.

In Fig. 6, the absorption coefficient initially rises and subsequently declines as the incident light energy increases. It reaches a maximum value near 12 eV, and the absorption coefficient is about 0 after 25 eV. Therefore, when the light intensity is greater than 25 eV, the propagation of the incident light in the $CuInSe_2$ will not be attenuated, and the crystal is transparent to this range of light.

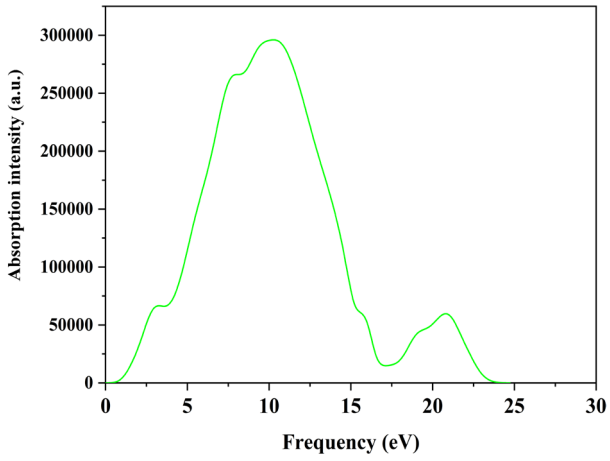

Fig. 6. Absorption coefficients of $CuInSe_2$.

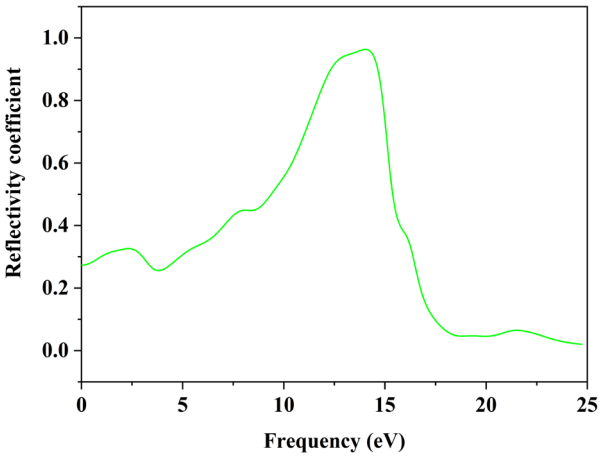

Fig. 7. Reflection coefficient of $CuInSe_2$.

The reflection spectrum of the $CuInSe_2$ is shown in Fig. 7. Fig. 7 reveals that the reflection coefficient remains minimal, at approximately 0.3, for incident light energies within the 0-5 eV range. With the increase of energy, the reflection coefficient gradually increases, reaches a maximum value near 15 eV, and then decreases rapidly. It approaches 0 at about 25 eV, which means that when the incident light with energy greater than 25 eV passes through the crystal, it is transparent.

The energy loss spectrum of $CuInSe_2$, derived from the calculations, is illustrated in Fig. 8. The incident light begins to have energy loss in the range of 15-23 eV, reaches the maximum energy loss at 16 eV, and has no energy loss outside this range.

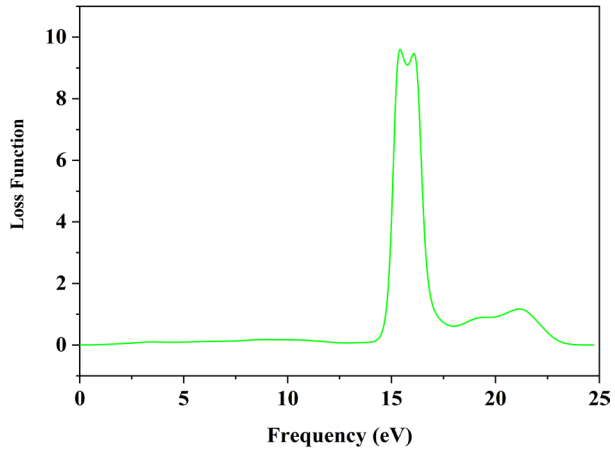

Fig. 8. Energy loss curves of $CuInSe_2$.

3.4. Elastic properties

The computed elastic constants alongside experimental and other theoretical values for comparative analysis is listed in Table 2. The table demonstrates that our calculated outcomes closely match the theoretical and experimental data[7, 17-20]. Therefore, the elastic constants of a stable

crystal have certain limitations. $CuInSe_2$ is a tetragonal crystal system, and the limitations for this crystal system are [16]:

$$C_{11}, C_{33}, C_{44}, C_{66}>0 \tag{4}$$

$$C_{11} > |C_{12}| \tag{5}$$

$$C_{11}C_{33} > C_{13}^2 \tag{6}$$

$$(C_{11} + C_{12})C_{33} > 2C_{13}^2 \tag{7}$$

Table 2. Theoretical and experimental values of C_{ij} (GPa), linear and bulk compressibility coefficients (TPa^{-1}), and anisotropy factors of $CuInSe_2$.

	This work	Theo. [17]	Theo. [7]	Theo. [18]	Theo. [19]	Exp.[20]
C_{11}	85.24	96.8	99.2	71	85.2	97
C_{12}	51.19	60.9	61.3	45	53.3	59.7
C_{13}	27.91	63.2	84.3	45.3	62.3	86
C_{33}	68.45	97.0	110.5	63	98.4	109
C_{44}	33.44	39.1	38.2	45	36.1	36
C_{66}	32.42	37.9	32.1	47	32.8	31.6
χ	20.78	13.52				
χ_a	5.21	4.62				
χ_c	10.36	4.28				
α_1	1.96	2.18				
α_2	0.97	0.97				

The calculated C_{ij} given in Table 2 meet the required stability criteria, suggesting that $CuInSe_2$ exhibits stability in its ground state. The two anisotropy factors α_1 and α_2 are:

$$\alpha_1 = 2C_{44}/(C_{11} - C_{12}) \tag{8}$$

$$\alpha_2 = C_{66}/C_{44} \tag{9}$$

It can be seen from the calculation results that α_1 and α_2 are quite different, indicating that the $CuInSe_2$ has strong elastic anisotropy.

The linear(volume) compressibility coefficients χ_a and χ_c (χ) can be calculated using the the following relationships[21]:

$$\chi_a = -\frac{1}{a}\frac{\partial a}{\partial p}\bigg|_{p=0} = S_{11} + S_{12} + S_{13} = \frac{C_{33} - C_{13}}{C_{33}(C_{11} + C_{12}) - 2C_{13}^2} \tag{10}$$

$$\chi_c = -\frac{1}{c}\frac{\partial c}{\partial p}\bigg|_{p=0} = S_{33} + 2S_{13} = \frac{C_{11} + C_{12} - 2C_{13}}{C_{33}(C_{11} + C_{12}) - 2C_{13}^2} \tag{11}$$

$$\chi = -\frac{1}{V}\frac{\partial V}{\partial p}\bigg|_{p=0} = 2\chi_a + \chi_c \tag{12}$$

The calculated linear compressibility coefficients of the $CuInSe_2$ along the *a* and *c* axes are χ_a = 5.21 TPa^{-1} and χ_c = 10.36 TPa^{-1} respectively, indicating that the influence of hydrostatic pressure on the compression in the two directions is consistent. The calculated value of the volume compressibility coefficient χ is 20.78 TPa^{-1}, these results align closely with values documented in existing literature [17].

The bulk modulus (*B*) is derived from C_{ij} using the Voigt-Reuss approximation [22-23]:

$$B_V = \frac{1}{9}(2C_{11} + C_{33} + 2C_{12} + 4C_{13}) \tag{13}$$

$$B_R = \frac{(C_{11} + C_{12})C_{33} - 2C_{13}^2}{C_{11} + C_{12} + 2C_{33} - 4C_{13}} \tag{14}$$

$$G_V = \frac{1}{15}(2C_{11} + C_{33} - C_{12} - 2C_{13} + 6C_{44} + 3C_{66}) \tag{15}$$

$$G_R = 15\left\{18B_V / C^2 + 6/(C_{11} - C_{12}) + 6/C_{44} + 3/C_{66}\right\}^{-1} \tag{16}$$

$$C^2 = (C_{11} + C_{12})C_{33} - 2C_{13}^2 \tag{17}$$

Finally, B and G can be obtained through the Hill method [24]

$$B = \frac{1}{2}(B_V + B_R) \tag{18}$$

$$G = \frac{1}{2}(G_V + G_R) \tag{19}$$

The B, G, and E show strong consistency with previously reported data[17]. The Poisson's ratio (σ) and Young's modulus (E) can be determined by the following formula:

$$\sigma = (3B - 2G)/(6B + 2G) \tag{20}$$

$$E = 9BG/(3B + G) \tag{21}$$

When the B/G of a material is above 1.75, it is deemed ductile; conversely, a ratio of 1.75 or less signifies a brittle material [25]. For the $CuInSe_2$, the B/G is 1.7428. The findings indicate that $CuInSe_2$ possesses excellent brittle, rendering it highly suitable for applications in mechanical processing.

Table 3. The B, G and E (GPa), σ, B/G of $CuInSe_2$.

	B	*G*	*E*	σ	*B*/*G*
This work	48.12	27.61	69.79	0.2637	1.7428
Theo.[17]	92.96	29.55	80.16	0.3563	

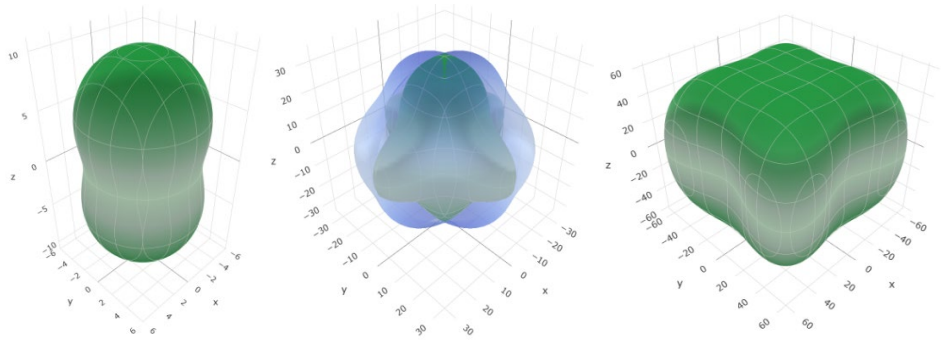

(a) *(b)* *(c)*

Fig. 9. Surface contours depicting the directional variations of (β) TPa^{-1} (a), (G) GPa (b), and (E) GPa (c) for $CuInSe_2$.

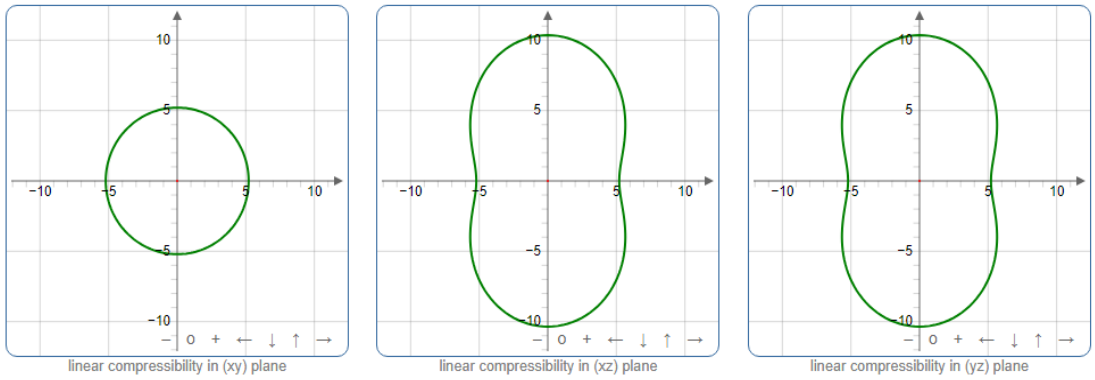

(a)

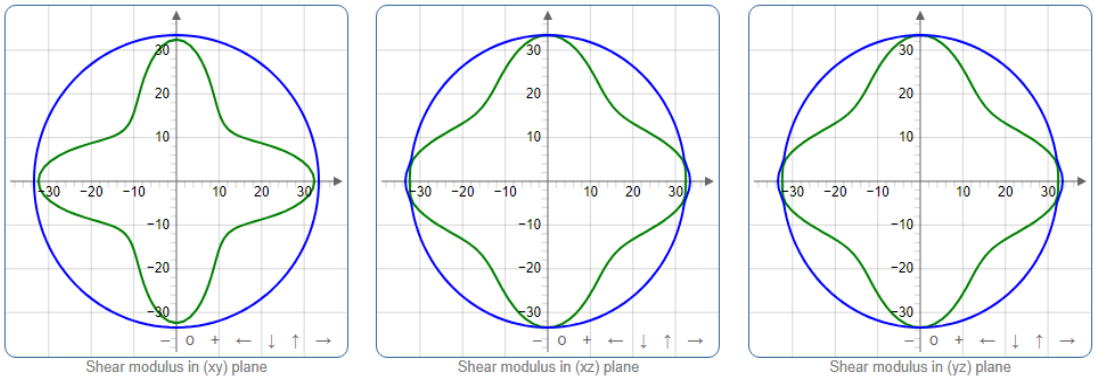

(b)

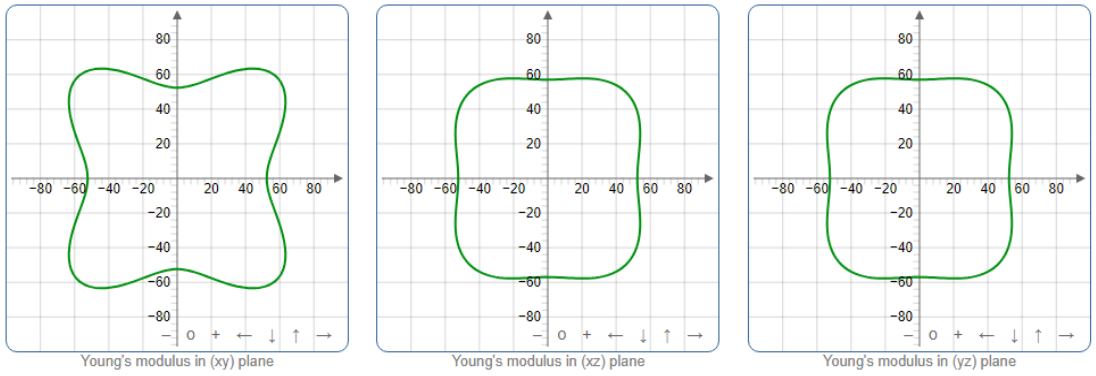

(c)

Fig. 10. Projections of β (TPa^{-1}) (a), G (GPa) (b) and E (GPa) (c) of $CuInSe_2$ in xy, xz, and yz planes.

Two-dimensional and three-dimensional graphical representations of linear compressibility (β), E, and G as effective means to illustrate the elastic anisotropy inherent in crystal structures[26]. Uniform circular and spherical graphical representations of crystals demonstrate their isotropic nature. Figs. 9 and 10 present the directional dependence of β, G, and E for $CuInSe_2$, displaying projections in the (xy)-, (xz)-, and (yz)-planes, as well as surface contour views, respectively. The elastic anisotropy of $CuInSe_2$ was quantitatively evaluated through the ratios β_{max}/β_{min}, G_{max}/G_{min}, and E_{max}/E_{min}. Higher values of these ratios indicate greater anisotropy. Specifically, the calculated

ratios are 1.9884 for β_{max}/β_{min}, 1.964 for G_{max}/G_{min}, and 1.586 for E_{max}/E_{min}, reflecting the material's anisotropic behavior.

4. Conclusions

In this work, the equilibrium structural parameters of $CuInSe_2$ were determined. $CuInSe_2$ exhibits the characteristics of a typical direct bandgap semiconductor. Analysis of its optical properties reveals key optical constants, including the dielectric function. For incident light energies exceeding 25 eV, the extinction coefficient of $CuInSe_2$ drops to zero, accompanied by a reflection coefficient of zero. Under these conditions, light undergoes complete refraction without attenuation, rendering the material fully transparent. The calculated elastic constants have an error of less than 15% compared with other theoretical values. When $\chi_a < \chi_c$, this indicates that the *a*-axis exhibits greater compressibility compared to the *c*-axis. α_1 and α_2 are quite different, that is, the $CuInSe_2$ has significant anisotropy. In addition, the ratio of *B*/*G* is 1.7428, indicating that it is a good brittle material.

Acknowledgments

This research was funded by the Technology Innovation Team of Yancheng Polytechnic College (YGKJ202503)

References

[1] P.Jackson, D. Hariskos, E. Lotter, S. Paetel, R. Wuerz, R. Menner, W. Wischmann, M. Powalla, Prog. Photovolt: Res.Appl.19, 894(2011); https://doi.org/10.1002/pip.1078

[2] R. P. Ingrid, A. C. Miguel, E. Brian, D. H. Clay, S. John, L. P. Craig, To. Bobby, Rommel Noufi, factor Prog.Photovolt: Res.Appl.16, 235(2008); https://doi.org/10.1002/pip.822

[3] S. E. DonLnelly, J. A. Hinks, P. D. Edmondson, R. D. Pilkington, M. V.Yakushev, R. C. Birteher, Nuclear Instruments and Methods in Physics Research Section B:Beam interactions with Materials and Atoms, 242, 686(2006); https://doi.org/10.1016/j.nimb.2005.08.089

[4] H. Liu, M.M.Yu, F.L. Qn, Feng, W, P.A. Hu, ACS Appl. Nano Mater. 1, 5414 (2019); https://doi.org/10.1021/acsanm.8b01527

[5] G. L. Chiu, T. Subburaj, S. Som, C.Y. Ou, C.H. Lu, J. Ceram. Process. Res. 18, 754 (2018)

[6] T. Gurel, R. Eryigit, Cryst. Res. Technol. 41, 83 (2006); https://doi.org/10.1002/crat.200410536

[7] A.K. Kushwahaa, C.-G. Ma, M.G. Brikb, S. Bin Omranf, R. Khenat, Mater. Chem. Phys. 227, 324(2019); https://doi.org/10.1016/j.matchemphys.2019.02.024

[8] Jose J. Plata, Victor Posligua, Antonio M. Márquez, Javier Fernandez Sanz, Ricardo Grau-

Crespo, Semiconductors Chem. Mater.34, 2833(2022); https://doi.org/10.1021/acs.chemmater.2c00336

[9] M. C. Payne, M. P. Teter, D. C. Allen, T. A. Arias, J. D. Joannopoulos, Rev. Mod. Phys. 64 (1992)1045; https://doi.org/10.1103/RevModPhys.64.1045

[10] J. P.Perdew, K. Burke, M. Ernzerhof, Phys. Rev. Lett. 77, 3865(1996); https://doi.org/10.1103/PhysRevLett.77.3865

[11] D. Vanderbilt, Phys. Rev. B 41, 7892 (1990); https://doi.org/10.1103/PhysRevB.41.7892

[12] A.V Postnikov, M.V Yakushev, Thin Solid Films 451-452 (2004)141; https://doi.org/10.1016/j.tsf.2003.11.005

[13] J. Feng, B. Xiao, J.C. Chen, Acta Physica Sinica, 56(10):5991(2007); https://doi.org/10.7498/aps.56.5366

[14] M.D Kannan, R. Balasundaraprabhu, S. Jayakumar, P. Ramanathaswamy Sol. Energ. Mat. Sol. C. 81, 379 (2004); https://doi.org/10.1016/j.solmat.2003.11.014

[15] H.J. Hou, W.X. Chen, S.R. Zhang, Q.F. Zhang, L.H. Xie, Int. J. Refract. Met. H. 113,106216 (2023); https://doi.org/10.1016/j.ijrmhm.2023.106216

[16] Born M, Huang K. England:Oxford Clarendon Press, (1954).

[17] Parlak C, Eryigit R., Phys. Rev.B, 73, 245217(2006); https://doi.org/10.1103/PhysRevB.73.245217

[18] J. Lazewski, H. Neumann, P.T. Jochym, K. Parlinski, J. Appl. Phys. 93,3789 (2003); https://doi.org/10.1063/1.1556179

[19] A.S. Verma, Sheetal Sharma, R. Bhandari, B.K. Sarkar, V.K. Jindal, Mater. Chem. Phys. 132,416 (2012); https://doi.org/10.1016/j.matchemphys.2011.11.047

[20] R. Fouret, B. Hennion, J. Gonzalez, S.M. Wasim, Phys. Rev. B 47,8269 (1993); https://doi.org/10.1103/PhysRevB.47.8269

[21] Neumann H, Cryst. Res. Technol. 39, 939 (2004); https://doi.org/10.1002/crat.200410280

[22] W. Voigt, Handbook of Crystal Physics, Taubner, Leipzig, 1928.

[23] A. Reuss, Z. Angew. Math. Mech 9 ,49(1929); https://doi.org/10.1002/zamm.19290090104

[24] R. Hill, Proceedings of the Physical Society. Section A, 65,349(1952); https://doi.org/10.1088/0370-1298/65/5/307

[25] S. F. Pugh, Philos. Mag. 45, 823 (1954); https://doi.org/10.1080/14786440808520496

[26] R. Gaillac, P. Pullumbi, F. X. Coudert, Journal of Physics: Condensed Matter, 28, 275201(2016); https://doi.org/10.1088/0953-8984/28/27/275201